

Development status of the differential accelerometer for the MICROSCOPE mission

D. Hudson ^{*,1}, R. Chhun, P. Touboul

Département Mesures Physiques, Office National d'Etudes et de Recherches Aéronautiques, BP72, 92322 Chatillon, France

Received 29 October 2004; received in revised form 26 September 2005; accepted 23 October 2005

Abstract

Tests of the Equivalence Principle are essential to fundamental physics theories, but as performed previously with torsion balances and laser ranging they have been limited by the vibrations inherent to any Earth-based environment. The MICROSCOPE mission will take advantage of the space environment to extend the EP test accuracy to 10^{-15} , by placing two masses of different materials in a drag compensated orbit. A violation of the Equivalence Principle will appear as a difference in the electrostatic forces necessary to maintain both masses on the same orbit. The satellite will be launched in 2008 and carry as the primary science instrument a differential electrostatic accelerometer.

The accelerometer is composed of two coaxial cylindrical proof masses surrounded by silica cages, in a vacuum housing. The two proof masses, one in platinum–rhodium within one in titanium, are maintained at the centre of their cages using electrodes engraved in the silica cage. These electrodes are used to capacitively sense the proof-mass position and to apply electrostatic forces to control the position. The accuracy and stability of the silica cage is therefore essential to the quality of the EP test.

This paper presents the current design of the accelerometer, specifically the critical areas for the instrument design, integration, and final performance requirements. Also discussed is the status of the analytical and theoretical models, as well as the experimental investigations, which are developed to overcome these critical areas.

© 2005 COSPAR. Published by Elsevier Ltd. All rights reserved.

Keywords: Space accelerometer; Electrostatic accelerometer; Equivalence principal; MICROSCOPE

1. Introduction

In 1911 Einstein proposed his Principle of Equivalence, postulating the equality of gravitational mass and inertial mass. In the years since this theory has been tested using numerous methods (Everitt et al., 2003), but the noise and vibrations inherent in any Earth-bound test environment have restricted the test accuracy (the Eötvös parameter) to no better than several 10^{-13} (Baessler et al., 1999). While free fall tests can avoid these noise issues, the test duration is too short (approximately 4 s in the Bremen facility) to achieve the sensitivity desired. Recent efforts

to obtain a unification theory of fundamental forces have renewed interest in disproving the Equivalence Principle (EP); for example, modern string theories predict an EP violation between 10^{-12} and 10^{-24} (Fayet, 2003). Present day satellite technologies are enabling EP tests to be performed this range, beginning with MICROSCOPE, which will reach 10^{-15} (Touboul et al., 2001). Potential future missions include the Galileo-Galelei (GG) mission (Nobili et al., 2000), proposing 10^{-17} , and STEP (Mester et al., 2004), which targets 10^{-18} .

Performing this test in space greatly reduces the experiment noise. In addition to removing the seismic vibrations of an Earth-bound lab, the space environment allows the measurements to be integrated over many orbits to reject other noise. Furthermore, remaining vibration sources are reduced by the drag compensating satellite control system. Performing this test in space offers another

* Corresponding author. Tel.: +33 1 46 73 47 88.

E-mail addresses: danya.hudson@onera.fr (D. Hudson), ratana.chhun@onera.fr (R. Chhun), pierre.touboul@onera.fr (P. Touboul).

¹ With support from the Centre National d'Etudes Spatiales.

advantage besides low noise levels: the frequency at which an EP violation may appear is well known, being the sum of the orbit frequency and the frequency of any spin of the measurement axis in the orbit plane.

The MICROSCOPE mission (French acronym for MICROSatellite à traînée Compensée pour l'Observation du Principe d'Equivalence) has been approved and funded under the CNES (Centre National d'Etudes Spatiales) MYRIADE microsatellite program which results in certain constraints on the payload. The MYRIADE satellites are a 1 m cube on launch, with a mass of 35 kg and power of 40 W allotted to the payload. As a result, MICROSCOPE will use two differential accelerometers that operate at ambient temperature, as cryogenics can not be accommodated within these restrictions. One instrument will contain proof masses of two different materials for the EP test, while the other will have two masses of the same material to provide a science baseline. The entire satellite will be within a 1 m cube on launch, with solar panels to be deployed once in its nearly circular ($e < 5 \times 10^{-3}$), 700 km altitude, heliosynchronous orbit.

The test concept is to place two test masses of different materials on precisely the same orbit, with mass centres within 10^{-11} m, and maintain them on this orbit by means of electrostatic forces. A difference in the forces required, due to a difference in the effect of gravity on the masses, will indicate an EP violation. The experiment will be performed on the two instruments, as mentioned above, but it will also be performed in two modes, inertial and spin, in order to perform the test at a range of frequencies within the accelerometer operating range of 10^{-4} to 1 Hz. In spin mode, a constant rate of spin is applied to the satellite by the drag-free attitude control system. The spin is about the common y axis of the instruments, with the resulting rotation in the orbit plane, as shown in Fig. 1.

The SAGE (Space Accelerometer for Gravitation Experimentation) accelerometer for MICROSCOPE is based on a successful heritage of high sensitivity electrostatic accelerometers developed by ONERA, including STAR, used on the CHAMP mission (Reigber et al., 2002), and SuperSTAR, for the GRACE mission (Davis et al., 1999). The differential accelerometer, however, is a step away from previous instruments due to the necessity of positioning two proof masses with a common centre of mass. This paper provides a detailed description of the SAGE instrument followed by a discussion of various design details critical to reach the targeted 10^{-15} accuracy. Section 4 provides an overview of the ground-based testing process. Details of the required in-orbit calibration requirements can be found in Guiu et al. (2005) in this issue.

2. The differential electrostatic accelerometer

An electrostatic accelerometer consists, fundamentally, of a proof mass (PM) suspended in a highly stable electrode cage. The principle of operation is to measure the electrostatic forces required from the electrodes to maintain the

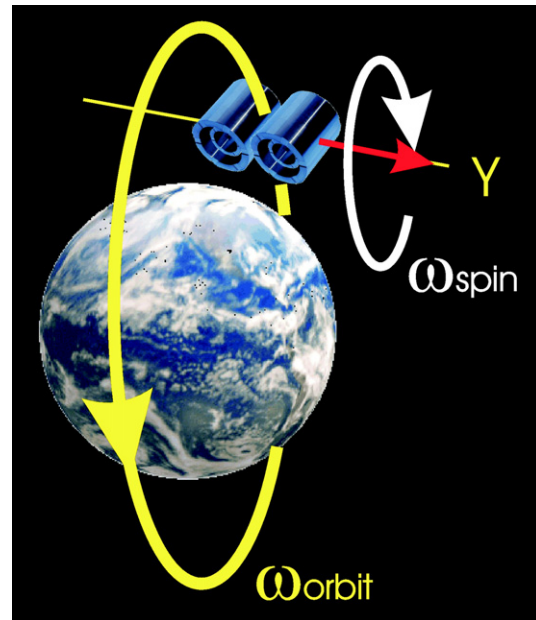


Fig. 1. The MICROSCOPE heliosynchronous orbit, with y pointing away from the sun. The measurement axis, x , is along the cylinder axes, while the y axis is through the centre of mass of the cylinders and satellite. The drag-free point will also be in line with the centres of mass, with the specific position depending on the measurement of interest.

position of the proof mass with respect to the cage. Because the suspended proof mass of a perfect sensor is susceptible only to gravitational forces and the electrostatic forces applied by the electrode cage, the force applied is proportional to the difference between the total acceleration of the cage and the gravitational acceleration of the proof mass. In the differential model, the two electrode cages experience the same acceleration, so that the differential measurement is the difference between the gravitational acceleration of the two masses.

There are three components to each SAGE instrument. The Sensor Unit (SU) contains the two inertial sensors carefully aligned in a vacuum tight housing. This is electrically connected to the Front End Electronics Unit (FEEU), which contains the low noise analogue electronics, including DACs, ADCs and position sensors, which require more thermal stability than the electronics of the Interface Control Unit (ICU). This latter unit contains the remaining electronics for SU operation, specifically the digital proof-mass position control loop, as well as the systems for general experiment control and the satellite interface.

2.1. Sensor unit mechanics

The objective of the MICROSCOPE mission is to compare the effect of gravity on two masses of different material, which requires subjecting them to the same gravitational field simultaneously. This requires precise alignment of the centre of mass of the proof masses, but also careful consideration of the shape of the mass to ensure the effects of gravity gradients are proportional between the two proof

masses. The SAGE instrument uses concentric cylindrical proof masses with dimensions chosen to produce equal moments of inertia (second order) on each axis. This has the advantage of preventing errors due to the effects of the gravity gradients while remaining a feasible shape for instrument design and accurate machining. With equal moments of inertia, the gravity gradient effects will be, to first order, independent of the PM orientation and therefore only proportional to its mass. This ensures that the effects of fluctuations in the self-gravitation of the satellite can be sufficiently cancelled from the differential measurement (Willemenot, 1997). Since the rotation of perfectly round cylinder about its axis cannot be detected, the SAGE proof masses have four narrow flat areas running the length of the outer surface of the cylinder to provide the required non-uniformity.

The sensor core of SAGE is therefore composed of two concentric, coaxial, cylindrical proof masses. The instrument providing the science base line has both masses in platinum–rhodium, while in the EP test instrument has the external mass in titanium and the internal in platinum–rhodium. The titanium mass has a nominal length of 79.9 mm, outer radius of 35 mm, and mass of 0.364 kg, while the smaller platinum mass has nominal dimensions of 43.51 mm in length, 20 mm in outer radius, and a mass of 0.473 kg. Each mass has a set of electrodes sufficient to control all six axes of motion (three linear, three rotational) engraved onto gold plated silica cylinders within and without the proof mass, so that the differential accelerometer is essentially one inertial sensor completely within the another as shown in Fig. 2. Hereafter the inertial sensors will be referred to as Sensors A and B, where Sensor A is internal to Sensor B.

The only physical contact on the proof mass is a thin gold wire, only 5 μm wide, which is essential to control the charge on the mass, which would otherwise vary throughout the mission. This wire is also used to apply a sinusoidal voltage to the PM to enable accurate position measurement. Three stops at each end of the PM cylinder limit its motion along and about the cylinder axis to prevent stress on the gold wire. At one end the stops are mobile to support the proof mass during launch but allow motion once in orbit (Section 3.4). Stops placed on the interior electrode prevent contact between the proof mass and electrodes, however, these stops are only necessary before control is obtained, or in the case of a loss of position control.

2.2. Electrodes

The same electrodes are used for both capacitive position sensing and electrostatic position control, and are arranged as shown in Fig. 3 to control all six degrees of freedom. The inner cylinder contains four independent pairs of electrodes for the two radial axes, y and z , and the rotations about these axes, ψ and θ . Linear measurements are provided by averaging the measurements from

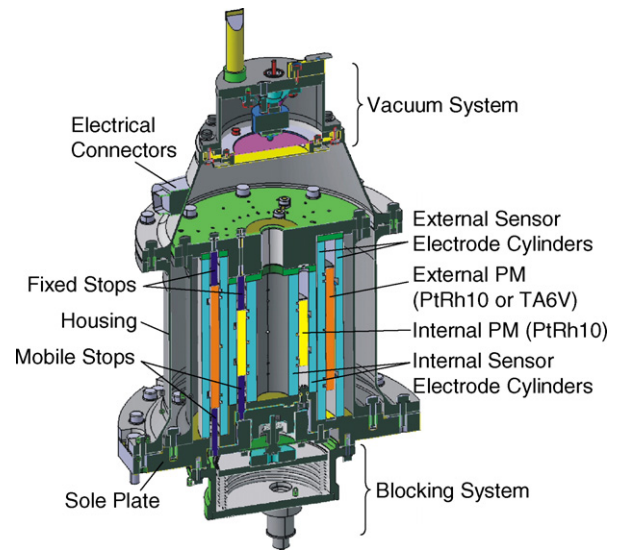


Fig. 2. Sensor unit cross-section. The cylindrical proof masses are shown in yellow and orange, each surrounded by two electrode cylinders in green. These are installed on the soleplate, which is specifically designed to guarantee a precise alignment. The blocking system is designed to retract the lower axial stops (three for each mass) after launch and the getter material in the vacuum system maintains a void of 10^{-5} Pa within the SU housing though the duration of the mission. (For interpretation of the references to color in this figure legend, the reader is referred to the web version of this paper.)

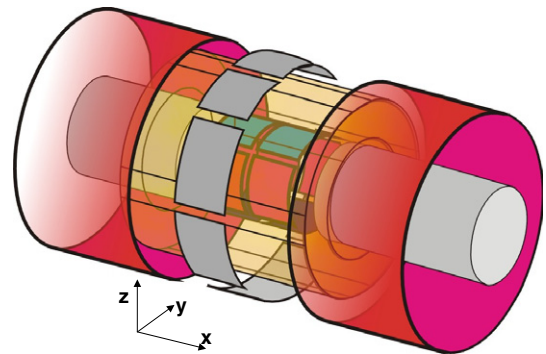


Fig. 3. Configuration of electrodes for proof-mass position measurement and control in six degrees of freedom. On the internal cylinder are four electrodes (green) on the vertical axis for z and θ , and four electrodes (red) on the horizontal axis for y and ψ . On the outer cylinder are the x electrodes (red) around the entire circumference, as well as a ring of eight electrodes (grey) for control in ϕ . (For interpretation of the references to color in this figure legend, the reader is referred to the web version of this paper.)

adjacent electrode pairs, while the rotational measurements come from the difference between adjacent pairs. The outer cylinder contains eight pairs of electrodes which act in unison for measurement and control of the rotation, ϕ , about the cylinder axis by means of the four narrow flattened areas on the outside of the proof masses. The electrodes for the sensitive axis, x , are also on the outer cylinder, covering the entire circumference at either end.

The cylindrical inertial sensor makes use of two capacitive techniques: variation of separation and variation of area. The variation of area method provides better linear control with less backaction from the detection signals for the sensitive axis, while the other axes use the variation of separation method typical of parallelepipedic accelerometers (Touboul et al., 1999). The cylindrical accelerometer is also much more complex than previous parallelepiped versions because the curvature results in a variation in separation across the electrode if the PM is not perfectly centred. This results in more complex equations, as the expressions for capacitance must be integrated over the area of the electrodes, and causes coupling between the axes (Lafargue, 2002) making position control more difficult.

Each electrode pair is connected to a capacitive position sensor. The difference in capacitance between the electrodes is proportional to the displacement of the proof mass with the relation defined by the geometry, and, for the sensitive axis, it is given by

$$G_{\text{det}_x} = \frac{2\epsilon\pi(R_{\text{co}} + R_{\text{mo}})}{e_o}. \quad (1)$$

For the radial electrodes, y and z , this is, to first order for each capacitive pair,

$$G_{\text{det}_y} = \frac{2\epsilon S_y \sin(\phi/2)}{e_i^2 (\phi/2)}, \quad (2)$$

where ϵ is the permittivity of free space, S is the electrode area, ϕ is the angular extent of the electrode, e is the separation between the electrode and proof mass when the PM is centred and R is the cylinder radius, with i and o subscripts indicating inner or outer and m and c subscripts indicating proof mass or electrode cylinder. These equations have been simplified by considering only small displacements of the proof mass along only the axis of interest. The resulting gains are listed in Table 1, with the corresponding free range of motion, as well as the measurement resolution of the position detector.

The same electrodes are used for position control by applying a voltage to each electrode. The resulting acceleration, Γ , can be expressed, using x for example, as

$$\Gamma_x = G_{\text{el}_x} V_x - \omega_{\text{p}_x}^2 x, \quad (3)$$

where G_{el_x} is the electrostatic gain defined by the SU geometry, V_x is the voltage applied to the electrodes, and $-\omega_{\text{p}_x}^2 x$

a destabilizing stiffness term, with x the PM displacement. Again assuming only small displacements along one axis, and neglecting coupling between the axes, the acceleration is proportion to the electrode voltage by

$$G_{\text{el}_x} = \frac{2\epsilon\pi(R_{\text{co}} + R_{\text{mo}})}{M e_o} V_p \quad (4)$$

for the sensitive axis, and

$$G_{\text{el}_y} = \frac{4\epsilon S_y \sin(\phi/2)}{M e_i^2 (\phi/2)} V_p \quad (5)$$

for both radial axes, where M is the mass of the PM, and V_p the PM polarization voltage. To first order the stiffness is

$$\omega_{\text{p}_x}^2 = 0 \quad (6)$$

for the sensitive axis, and

$$\omega_{\text{p}_y}^2 = \frac{2\epsilon S_y}{M e_i^3} \left(1 + \frac{\sin(\phi/2)}{(\phi/2)} \right) V_m^2 \quad (7)$$

for y and z , with V_m the total voltage on the PM, a combination of the polarization voltage and the sinusoidal detection voltage. Table 2 provides the numerical values of the gain and stiffness calculated from the SU dimensions. The proof mass voltage used to create this table is for the high resolution mode operation, with V_p a constant 5 V and V_d the sinusoidal component with an rms of 5 V.

2.3. Position control loop

The position control loop consists of a capacitive position sensor to determine the PM position and a digital set of control laws to control the PM position, as well as the necessary amplifiers, ADCs and DACs as illustrated in Fig. 4. The position sensor operates thanks to the sinusoidal voltage applied to the proof mass. This voltage induces a current from each electrode which is proportional to the capacitance between the PM and that electrode. A differential transformer then converts the difference in current between electrode pairs to a voltage proportional to the PM position.

This voltage from the capacitor detector is digitized and input to the control laws, which can be based on a standard PID loop. The control laws are developed by means of a Matlab model and will be verified and refined during ground testing. The parameters of the control laws will

Table 1
Capacitive sensing physical gains for each electrode pair, provided in pF/ μm for the linear axes and pF/mrad for the angular axes

Axis	Sensor A			Sensor B		
	Gain	Range	Resolution	Gain	Range	Resolution
x	7.47×10^{-3}	± 100	4.0×10^{-5}	6.55×10^{-3}	± 100	4.6×10^{-5}
y, z	-0.123	± 150	1.1×10^{-5}	-0.545	± 150	9.7×10^{-6}
θ, ψ	-0.953	± 12.0	1.4×10^{-6}	-8.59	± 4.3	5.9×10^{-7}
ϕ	3.76×10^{-2}	± 3.3	1.2×10^{-5}	9.20×10^{-2}	± 1.8	1.1×10^{-5}

As the ϕ electrodes are wired as one, the gain is provided for all four electrode pairs together. The range is provided in μm or mrad as appropriate, and the resolution in μm or mrad per $\sqrt{\text{Hz}}$, at the 7.8×10^{-4} Hz EP test frequency.

Table 2
First-order gain and stiffness parameters for the acceleration produced by the electrodes

Axis	Sensor A		Sensor B	
	G_{el}	ω_p^2	G_{el}	ω_p^2
X	-7.93×10^{-2}	0.00	-9.27×10^{-2}	0.00
Y, Z	2.61	0.137	15.4	0.812
θ, ψ	6.48×10^{-2}	2.63×10^{-2}	0.230	0.190
ϕ	1.28×10^{-3}	1.30×10^{-5}	1.23×10^{-3}	7.09×10^{-6}

The gain is provided in units of acceleration ($\mu\text{m}/\text{s}^2$ or mrad/s^2) per volt while the stiffness parameter is in Hz^2 .

be tailored to produce the same response from each inertial sensor, which is necessary for the differential measurement. Specifically, the response from both sensors must be in phase, with the same gain (preferably 1 at the EP frequency), and with a bandwidth greater than 4 Hz for effective drag-free satellite control. The output from the control loop is amplified and applied, with opposite signs, to both electrodes. With this voltage on the electrodes, and the DC component of the proof mass voltage controlled via the gold wire, an electrostatic force results which is proportional to the electrode voltage in this symmetric configuration.

When the proof-mass position is controlled stationary with respect to the electrodes, the force applied by the electrodes is proportional to the difference between the forces on the proof mass and the forces on the electrode cage (i.e., the satellite), namely the drag. The drag-free control system therefore uses the output from the control laws to compensate for the satellite drag. This output allows a large acceleration range, which is necessary before the drag-free control is operating. The EP test data from the sensitive axis, on the other hand, is sampled after the last amplifier in the loop in order to reject the noise from all components including the DAC and this drive voltage amplifier.

3. Mission critical design considerations

3.1. Alignment to gravity field

Mission specifications call for an alignment between the measurement axis and orbital plane to within a few thousandths of a radian to achieve the required test accuracy. This alignment is measured via a star camera and main-

tained by the electric thrusters of the drag-free control system. The actual attitude must be known to within 10^{-3} rad in order to correct for the effects of the gravity gradient in the differential measurement, and therefore the alignment of the sensor core to the star camera must be well known and very stable. The star camera and sensor units are precisely aligned during satellite integration via an optical cube on the SU base plate. The stability of this alignment is, however, dependent on the rigidity and thermal sensitivity of the satellite bus. The in-flight calibration phase provides a precise determination of the star camera to SU alignment (Guieu et al., 2005), which means reverification is possible during the mission. The sensor units themselves are carefully assembled and mounted on the base plate to provide precise alignment of the core cylinders with the optical cube, and the material of the sensor unit, primarily Invar with silica electrode cylinders, is chosen for its thermal stability.

3.2. Thermal stability

The thermal control in the microsatellite is performed entirely by passive methods, which is possible thanks to the heliosynchronous orbit which minimizes thermal variations. The satellite structure, developed by CNES, is designed to achieve the required thermal stability via insulation and radiators. The more sensitive SU and FEEU are insulated from the other satellite components to reduce temperature variability and the vacuum and double walled housing of the SU further insulates the core mechanics.

Thermal variations in both the electronics and mechanics produce corresponding variations in the bias and scale factors which relate the instrument output, in volts, to an acceleration measurement. Each axis of each inertial sensor has its own bias and scale which depend on various properties and components such as the cylindricalness of the proof mass, the capacitive position sensor, the electrode symmetricalness, the gold wire damping, and the drive voltage amplifier response. The effect of SU and FEEU temperature variations on each contributor to the bias and scale has been analysed, with the results summarized in Table 3 for a measurement frequency of 7.8×10^{-4} Hz (spin mode).

To maintain the performance requirement level of better than 8×10^{-15} m/s^2 , temperature variations at the test

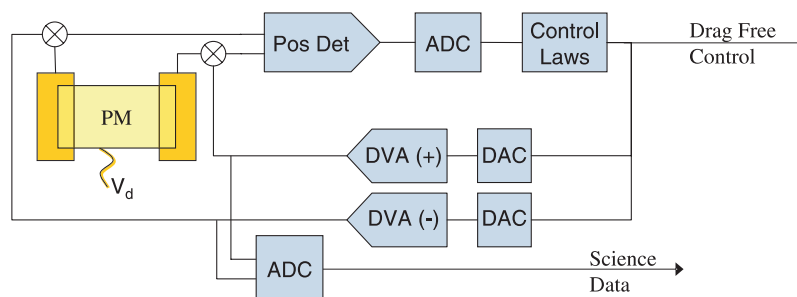


Fig. 4. Control loop for accelerometer operation along the x axis.

Table 3
Scale and bias variations for the sensitive axis, in $\text{m/s}^2/\text{K}$, due to thermal variations in the SU or FEEU

	SU	FEEU
Sensor A bias error	2.20×10^{-13}	3.27×10^{-14}
Sensor B bias error	3.09×10^{-13}	1.56×10^{-14}
Sensor A scale error	2.14×10^{-13}	7.06×10^{-14}
Sensor B scale error	1.63×10^{-13}	7.06×10^{-14}
Total error	9.06×10^{-13}	18.95×10^{-14}

To enable comparison, the bias errors are converted to units of acceleration (from acceleration per volt), using the voltage corresponding to the maximum measurable acceleration, $2.5 \times 10^{-7} \text{ m/s}^2$.

frequency are limited to $\pm 1 \text{ K}$ for the ICU, $\pm 10 \text{ mK}$ for the FEEU, and $\pm 1 \text{ mK}$ for the SU. The instrument temperature will be monitored via platinum resistors within the three components (currently four in the SU, three in the FEEU and two in the ICU) to allow refinement of the bias and scale parameters throughout the mission.

3.3. Instrument sensitivity

The maximum acceleration measurable by the accelerometer is $2.5 \times 10^{-7} \text{ m/s}^2$. The minimum detectable acceleration is dependent on the measurement frequency, and has been determined by analysing the sensitivity of each contributing component to determine which are the limiting factors. The resulting instrument sensitivity is displayed in Fig. 5 for the sensitive axis, and is defined by the limits of four contributors, the capacitive sensor, the readout electronics, the gold wire damping, and the thermal sensitivity of the bias.

The capacitive sensor defines the sensitivity at frequencies above about $2 \times 10^{-2} \text{ Hz}$. The noise of the capacitive sensor circuit, n_c , is $7.5 \times 10^{-6} \text{ V}/\sqrt{\text{Hz}}$ in this frequency range, and is converted to an instrument sensitivity by $\omega^2 n_c / G$, where G is the gain defined by the voltage range of the electronics, and for this analysis taken as $0.25 \text{ V}/\mu\text{m}$.

At lower frequencies, below $3 \times 10^{-3} \text{ Hz}$, the gold wire damping becomes the contributing factor. F. Bourdonneau² has experimentally measured the effects of a 1.7 cm length of $5 \mu\text{m}$ gold wire to find a damping, H , of less than $6.25 \times 10^{-7} / \omega \text{ Ns/m}$. SAGE uses the same wire, but 2.5 cm long. To adapt for the length, the $1/\text{length}^3$ dependence of the wire stiffness, k , is used with the relation $H = k/Q\omega$, under the assumption that the same quality factor, Q , is valid for both cases. This gives a damping estimate for the SAGE wire of $1.96 \times 10^{-7} / \omega \text{ Ns/m}$, which is then converted to a sensitivity by $\sqrt{4k_b T H / M}$ (Nyquist noise), where k_b is Boltzmann's constant, T is the nominal SU temperature, and M is the mass of the PM.

Between these is the range of best sensitivity of less than $4 \times 10^{-13} \text{ m/s}^2/\sqrt{\text{Hz}}$, which is defined by the electronics of the readout circuit. The noise of the control loop compo-

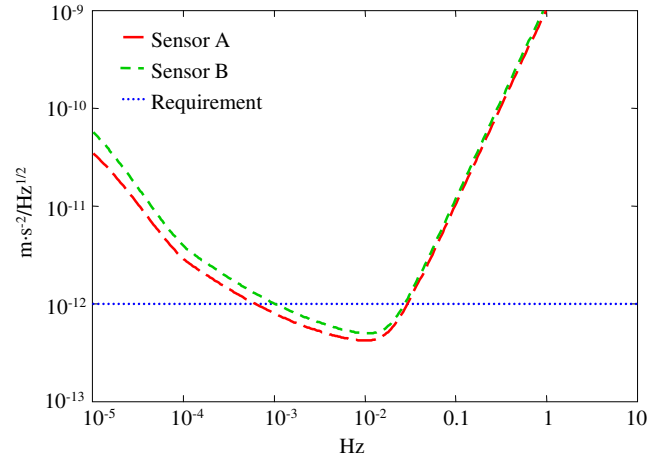


Fig. 5. Instrument sensitivity for the axial measurements.

nents are effectively rejected by sampling the data after the last component (the DVA), but the sampled data are digitized and amplified, and these two components are an additional noise source. The noise of the ADC and gain of the amplifier are combined and converted to an instrument sensitivity via the electrostatic gain.

The thermal sensitivity of the bias is the lowest frequency contributor, taking effect below 10^{-4} Hz . This is below the lowest possible frequency for the EP test, which is the orbit frequency when operating in inertial mode (see Section 1). However, to complete the sensitivity characterization, the thermal sensitivities of the components contributing to the bias are analysed and converted to a sensitivity via the appropriate thermal stability, either $3 \text{ K}/\sqrt{\text{Hz}}$ for the electronics or $0.3 \text{ K}/\sqrt{\text{Hz}}$ for the SU.

Considering a signal integration time of 20 orbits, a sensitivity of better $2 \times 10^{-12} \text{ m/s}^2/\sqrt{\text{Hz}}$ is required to achieve the targeted 10^{-15} test accuracy. At the test frequency for the first planned spin mode, $7.8 \times 10^{-4} \text{ Hz}$, the sensitivity is just attained. Fig. 5 shows that the outer sensor is just over target, at $1.1 \times 10^{-12} \text{ m/s}^2/\sqrt{\text{Hz}}$, but the inner sensor is sufficiently under target to compensate. With a foreseen integration time of $1.2 \times 10^5 \text{ s}$ the differential signal at this frequency will have a maximum sensitivity of 6×10^{-16} . A much longer integration time is required to reach the same sensitivity at the lower frequency of the inertial mode, with a 120 orbit integration currently being considered.

3.4. Launch stress durability

To attain the desired performance in orbit, the instrument must withstand the launch vibrations. To avoid damage to the sensor unit by the proof mass, each mass is supported by three stops at each end of the cylinder. At one end a blocking system applies 2400 N to the three stops during launch to prevent slippage between the stops and proof mass, and once in orbit it retracts the stops a few microns to allow SU operation. A preliminary analysis has been performed via numerical modelling to determine how much movement the stops permit. With the expected

² PhD student at ONERA, thesis to be published spring 2006.

maximum acceleration during launch of 20 g applied, in a uniform direction normal to the cylinder axis, to the proof mass and all six stops, the maximum displacement with any orientation of the three stops was found to be 23.4 μm for the most massive PM, the external platinum mass. As the smaller separation between the proof mass and internal cylinder is 145 μm , this is considered a safe amount of motion. A complete verification of the blocking system design will be obtained through vibration testing of the flight qualification test model.

A second analysis is also in progress to calculate the electrostatic effects of the stops after they are retracted. The tip of each stop must be held at the same voltage as the proof mass in order to avoid electrostatic forces between the two, while the sides of the stops will be electrostatically shielded to minimize perturbations of the capacitive measurement. However, there will be a small parasitic capacitance between the stops and electrodes and the numerical analysis is required to verify that this effect is negligible.

Besides providing sufficient support to the proof mass, the greatest concern for the blocking system design is that the proof mass can be released without the stops sticking to or otherwise damaging it. The three stops at each end are aligned with three slight (1 μm deep) indentations in the proof mass. This geometry limits the contact between the stop and the PM to a ring along the bevelled edge of the indentation. However, the resulting concentrated force will likely produce a deformation of the proof mass. This could produce a compression of the PM material, which would have a minimal effect on the proof mass moment of inertia. Alternatively, some of the compressed material may remain stuck to the stop when it is retracted, which may have a more significant effect. In addition to the mechanical effects, surface deformation or any other disturbance to the gold coating of the PM surface could alter the electrical properties of the SU. However, such effects are minimized because the bevelled edge of the indentation does not directly face any of the electrodes.

4. Ground testing

The highly sensitive accelerometer requires the micro-gravity environment of Earth orbit for suspension of the proof masses. As a result, the instrument optimized for in-flight operation cannot be fully tested prior to flight. Instead, pre-flight testing is performed by means of test models adapted for operation on ground. The ground test campaign involves operating the various test models via artificial levitation and via free fall testing at the Bremen Drop Tower. Preliminary tests to verify the ability to control of a cylindrical proof mass will be performed on a specialized levelling bench, while further testing to optimize control loop parameters and verify the expected performance levels will make use of a low noise pendulum bench. The drop tower will be used to perform tests with both the development and flight models which cannot be performed with artificial levitation.

Operation of the test models on ground (outside of free fall) requires counteracting the force of gravity by applying a high voltage to electrodes on the vertical axis, which is further facilitated by adaptations of the test model, namely the use of light-weight silica proof masses. The prototype model used for proof of concept (the premier levitation of a cylindrical proof mass), contains only one inertial sensor and has very small separation between the silica proof mass and electrodes (40 μm). As well, four phi electrodes above and below the proof mass are replaced by two larger supplemental electrodes to assist with levitation. To counteract gravity, approximately 425 V will be required on the lower z electrodes and the upper supplementary electrode when the proof mass is centred. The remaining vertical electrodes are maintained at V_p to match the PM voltage and avoid increasing the downward force. However, elevated voltages are required on other electrodes as well, due to the instability of the configuration, as well as uncertainty of the alignment with the local gravity field, coupling between the axes, and uncertainties in the SU geometry.

The initial alignment of the z axis to the local gravity field is limited by the alignment of the sensor core to its support structure, the levelling of the test bench and the assumption that the local gravity field is vertical. On the levelling bench used for the initial levitation with the prototype, the initial alignment of the sensor can be achieved to within an estimated 1 mrad of the local gravity field, and therefore elevated voltages may be required on the electrodes of the other axes. For example, a 1 mrad misalignment in the x - z plane is equivalent to a 1.37×10^{-4} N force due to gravity on the x axis, which corresponds to a voltage of 117 V required on the x electrodes for levitation. Once the proof mass is levitated, the alignment can be improved by adjusting the position to minimize the voltage required on the x and y electrodes. However, more sensitive measurements will be performed using a pendulum bench, which naturally compensates for the local gravity field and reduces environmental noise.

Coupling between the measurement axes occurs in a cylindrical accelerometer due to the variation in separation over the curved electrodes when the proof mass is not perfectly centred. A displacement can affect the radial axes, while additional rotation affects the sensitive axis as well, as discussed in Lafargue (2002). Because the proof mass is initially far from centre and the high voltage is applied asymmetrically to the z electrodes (to the lower electrodes only), axis coupling is a greater concern before the artificial levitation has stabilized. However, the nominal position may also not be a perfect alignment with the electrode cylinders. Misalignment between the two electrode cylinders can result in an offset of the proof mass with respect to the outer cylinder, as the alignment of the proof mass axis is controlled by the radial electrodes on the internal cylinder. As well, dissymmetries in the electrode pairs can produce proportional errors in the capacitive position determination which result in a displaced proof mass. These dissymmetries can also cause coupling between forces applied to the linear and rotational axes.

Another source of axis coupling is faults in the cylindricality of the various cylinders. The requirements for the flight model are specified in terms of the maximum variation in diameter over the length of the cylinder and are 2 and 5 μm for the proof mass surfaces and electrode cylinders, respectively. In the worst case scenario, the four surfaces would be slightly conical, and the x electrodes would cause an offset of the proof mass along its axis. However, the more significant effect is the coupling which would be produced between the radial electrodes and the sensitive axis. When the high voltage is applied for artificial levitation a vertical force is created to balance out gravity, but the angle of the components in this worst case scenario creates a force of about 0.02% of gravity along the x axis. To compensate, another 20 V would be required on the x electrodes to achieve levitation.

The accelerometer test models can be operated on ground by applying a high voltage on the z electrodes to produce an artificial levitation of the proof mass, but with significantly reduced performance. The increased voltage required on the x electrodes, even when perfectly horizontal, decreases the resolution on the sensitive axis, and decreases the linearity if the PM is not perfectly centred. In addition, the coupling of the axes results in a projection of the gravitational noise onto the x axis. An electrostatically controlled pendulum can reduce the noise on the horizontal axis to $10^{-8} \text{ m/s}^2/\sqrt{\text{Hz}}$ below 0.1 Hz, however, above this frequency it remains at about $10^{-6} \text{ m/s}^2/\sqrt{\text{Hz}}$ (Touboul et al., 1998). Free fall testing allows operation without the high voltage levels, but the measurement duration (4.7 s at Bremen) limits the noise rejection possibilities. A low noise double capsule is under development to accommodate SAGE testing, which currently achieves noise levels of $10^{-7} \text{ m/s}^2/\sqrt{\text{Hz}}$ in the 0.2–10 Hz bandwidth.

5. Conclusion

To test the Equivalence Principle to a precision of 10^{-15} , a differential electrostatic accelerometer is in the process of development. This accelerometer maintains two concentric coaxial cylindrical proof masses on a common orbit with electrostatic forces, and any difference in the required force indicates a difference in the effect of gravity. Performing this test in space offers many advantages, including knowledge of the frequency at which a violation will appear. This frequency can be chosen by spinning the satellite in its orbit plane.

The precision and stability of both the mechanical and electrical systems are essential to achieve the targeted 10^{-15} EP test accuracy. The precision of the mechanical system is achieved through exact machining and careful alignment during assembly of the sensor unit and the satellite, and to ensure the SU reaches orbit without damage, a blocking system has been designed to support the proof masses through the stresses of launch. The stability of mechanical alignments and electronic responses is achieved through the use of materials with low temperature sensitivities and the requirement of low thermal variations on the

satellite. The resulting error due to temperature change is well within the target limits. The instrument sensitivity is also essential to reach 10^{-15} , and although a much longer integration time will be required when the satellite attitude is fixed in inertial space, the spin mode increases the EP frequency to a range with a sensitivity sufficient for the expected 20 orbit integration duration.

The final flight model, which is optimized for operation in orbit, cannot be fully tested on ground due to the inherent environmental noise and the magnitude (1 g) and variability of the local gravity field. However, a series of development models are adapted for ground testing, which is possible via artificial levitation on a specialized levelling bench or low noise pendulum apparatus, or via the low gravity in free fall at the Bremen Drop Tower. The performance of the pre-flight models will be used to anticipate the flight model characteristics, and to define the constraints required to achieve the 10^{-15} EP test accuracy.

Acknowledgements

The authors recognize Sylvie Leon, Jean-Bernard Dubois, and their group at CNES for their support.

References

- Baessler, S., Heckel, B.R., Adelberger, E.G., et al. Improved test of the equivalence principle for gravitational self-energy. *Phys. Rev. Lett.* 13, n18, 1999.
- Davis, E.S., Dunn, C.E., Stanton, R.H., Thomas, J.B. The GRACE mission: meeting the technical challenges, in: 50th International Astronautical Congress, IAF-99-B.2.05 Conference, AAS 90-034, 1999.
- Everitt, C.W.F., Damour, T., Nordtvedt, K., et al. Historical perspective on testing the equivalence principle. *Adv. Space Res.* 32 (7), 1297–1300, 2003.
- Fayet, P. Theoretical motivations for equivalence principle tests. *Adv. Space Res.* 32 (7), 1289–1296, 2003.
- Guiu, E., Rodrigues, M., Touboul, P., Pradels, G. Calibration of MICROSCOPE, *Adv. Space Res.*, in press, 2005.
- Lafargue, L. Configuration mécanique d'accéléromètres électrostatiques pour le test en orbit du principe d'équivalence, Ph.D. Thesis, Université Paris VI Pierre et Marie Curie, Chapter III-4 (in French), 2002.
- Mester, J., Buchman, S., Cruise, A.M., et al. Gravitational experiments in space: gravity probe B and STEP. *Nucl. Phys. B Proc. Suppl.* 134, 147–154, 2004.
- Nobili, A.M., Bramanti, D., Polacco, E., et al. The Galileo Galilei (GG) project: testing the Equivalence Principle in space and on Earth. *Adv. Space Res.* 25 (6), 1231–1235, 2000.
- Reigber, C., Luehr, H., Schwintzer, P. CHAMP mission status. *Adv. Space Res.* 30 (2), 129–134, 2002.
- Touboul, P., Foulon, B., LeClerc, G.-M. STAR, the accelerometer of the geodesic mission CHAMP, in: 49th International Astronautical Congress, IAF-98-B.3.07 Conference, 1998.
- Touboul, P., Willemenot, E., Foulon, B., Josselin, V. Accelerometers for CHAMP, GRACE and GOCE space missions: synergy and evolution. *Boll. Geof. Teor. Appl.* 40, 321–327, 1999.
- Touboul, P., Rodrigues, M., Métris, G., Tatry, B. MICROSCOPE, testing the equivalence principle in space, *C.R. Acad. Sci. Paris IV* 2 (9), 1271–1286, 2001.
- Willemenot, E. Pendule de torsion à suspension électrostatique, très hautes résolutions des accéléromètres spatiaux pour la physique fondamentale, Ph.D. Thesis, Université de Paris-Sud U.F.R. Scientifique d'Orsay, Ch 1-C, 1997 (in French), 1997.